Organic Electronics 13 (2012) 905–913

Contents lists available at SciVerse ScienceDirect

Organic Electronics

journal homepage: www.elsevier.com/locate/orgel

Quantitative characterization of carrier injection across metal–organic interfaces using Bardeen theory

Mohammad-Reza Fathollahi [a,*], Farhad Akbari Boroumand [a], Farshid Raissi [a], Mohammad-Javad Sharifi [b]

[a] Faculty of Electrical and Computer Engineering, K.N. Toosi University of Technology, P.O. Box 16315-1355, Tehran 1431714191, Iran
[b] Faculty of Electrical and Computer Engineering, Shahid Beheshti University, G.C., Evin, Tehran 19839, Iran

ARTICLE INFO

Article history:
Received 23 October 2011
Received in revised form 28 January 2012
Accepted 29 January 2012
Available online 11 February 2012

Keywords:
Carrier injection
Organic devices
Bardeen tunnelling theory
Hopping rate
Polyfluorene

ABSTRACT

We have investigated the contact between a metal and an organic/polymeric (o/p) material and we have introduced a relation for carrier injection using Bardeen theory. A series of narrow barriers is considered in the semiconductor side to account for the localized nature of the carriers in the o/p material. As an application of the model, we have calculated the hopping rate of carriers in terms of the contact parameters. Also, we have discussed the hopping of carriers deep into the organic dielectric. Finally, we have explored the hopping rate in practical contacts between polyfluorene-based polymers and different electrodes.

1. Introduction

Theoretical study and modelling of the physical mechanisms in organic devices is of prime importance to enhance the device functionality [1–6]. Current injection across the contact has been proven to have significant effect on device characteristics [7]. Energy difference between the Fermi level of the electrode and the lowest unoccupied molecular orbital (LUMO) or the highest occupied molecular orbital (HOMO) of the organic semiconductor forms an injection barrier at the contact.

Clear understanding and modelling of contact between the metal (m) and the organic/polymeric (o/p) semiconductor is not straightforward task to follow [7]. For instance, even interfaces such as Ca/Alq_3 (tris-8-hydroxyquinolato aluminium) with no energy difference do not behave ohmic [8,9]. The first cause of this difficulty is the different nature of the carrier transport in organic materials in comparison with the common semiconductors. Indeed, the parameters of the contact would differ dramatically as they can be affected by several causes such as the conditions in which the sample prepared and the variety of the materials which can be used. Also, the chemical reaction and interface chemistry can considerably change and control the injection process across the contact [10].

Conventionally, the injection current in organic devices is described by Fowler–Nordheim tunnelling, Richardson–Schottky thermionic emission, and taking into account the backflow interface recombination [7,9,11]. Furthermore, the effect of low mobility in organic semiconductors can be considered using the thermionic emission–diffusion theory of Crowell and Sze [11,12].

Nonetheless, employing these models in organic devices is quite questionable as the nature of transport is different in them; therefore, there have been several efforts to bring some more realistic explanations. For instance, Arkhipov and co-workers proposed a model describing the injection as an initial hopping of carriers from the Fermi level in metal into the electronic states of the organic material

* Corresponding author. Tel.: +98 21 88462174x406; fax: +98 21 88462066.
E-mail addresses: fathollahi@ee.kntu.ac.ir, m.r.fathollahi@gmail.com (M.-R. Fathollahi).

1566-1199/$ - see front matter © 2012 Elsevier B.V. All rights reserved.
doi:10.1016/j.orgel.2012.01.029

followed by diffusive escape from the image potential [1,13]. This model takes into account the energetic disorder in the dielectric by considering a Gaussain distribution. However, more studies have been carried out to describe the electrical and temperature dependency of the injection in better agreement with the experiments. For instance, Yang and co-workers considered conducting filaments formation for proper modelling of the injection at low bias voltages [9]. Moreover, Baldo and Forrest demonstrated that to address the low temperature characteristic of the injection properly, and the power-law behaviour, it is essential to take into account the effect of interfacial dipoles on broadening the energy distribution [14]. In latter study, they modelled the injection by considering the polaron hopping. Indeed, they determined the unknown parameters by fitting the modelling results with the experimental data. Earlier, Bussac et al. considered all the effects such as external field, space charges, and image force in their model. They obtained the polaron hopping rate and the current injection by calculating the overlap between the evanescent wave function in the metal and the proper extended state of the polymer [12]. In particular, they explored the Coulomb trapping of the bipolarons in the generalized image potential and its effect on increasing the schottky barrier at the interface. Later, they expanded their injection relation by including a decay factor related to the intermolecular tunnelling [15].

The present brief review of the literature demonstrates there have been different approaches so far trying to describe the injection in organic devices. Occasionally, these models get quite sophisticated. Moreover, there are some parameters in these methods that their values are typically estimated by data fitting between modelling and experiment. Some examples are v_0 the hopping rate [1,9,13], J_0 the intermolecular overlap integral [14], gm the tunnelling parameter between the electrode and the first molecular monolayer [15].

In present paper, by considering only the major features of an organic-conductor junction in a quantum-mechanics problem, we present a simple method for derivation of an injection relation describing the carrier transfer. Mainly, we consider the localized nature of the carriers in the organic material and equivalently the presence of the narrow barriers between each pair of nodes in the one-dimensional potential profile. We formulate the carrier dynamics in an appropriate form by using Bardeen tunnelling theory and we calculate the carrier hopping rate quantitatively. Also, we investigate the direct hopping of carriers deep into the organic semiconductor.

In Section 2 , we introduce Bardeen theory following Gottlieb and Wesoloski [16]. In Section 3, we apply the theory to calculate the carrier transfer between two subsystems containing band-like states. It points out the compatibility of Bardeen method with the standard tunnelling theory. Also, the result from this section in comparison with the result for the metal–organic contact (Section 4) clarifies the effect of the localized states. In Section 4, we derive a relation for carrier injection across metal–organic contact. Afterwards, in the last section, we examine the validity of the theory by using the presented relation to model the current density–voltage (J–V) characteristic of PFO-based OLEDs. Finally, we present a quantitative investigation concerning hopping frequency for practical contacts. It includes the dependency of the hopping rate on the height and width of the barrier. Also, we discuss the injection deep into the organic dielectric.

2. Bardeen tunnelling approach

Five decades ago, Bardeen presented a theory to characterize tunnelling current between two systems separated by a potential barrier [17]. To develop the theory, he assumed the tunnelling caused by scattering events that transfer the carrier across the barrier [16]. Bardeen theory has been used successfully to describe phenomena such as tunnelling current between a scanning tunnel microscope (STM) tip and a sample [16,18,19], electron transmission through molecular structures [20], and tunnelling in a metal oxide semiconductor (MOS) structure [21].

Considering a potential profile illustrated in Fig. 1a and assuming a particle placed in one side of the potential, the objective is to find the tunnelling probability and the particle occupation on the other side of the system. The total Hamiltonian, H_{tot}, and its corresponding wave function, $\psi(x,t)$, satisfy the Schrödinger equation below:

$$H_{tot}^{tun}\psi(x,t) = -\frac{\hbar^2}{2m}\nabla^2\psi(x,t) + V(x)\psi(x,t) = i\hbar\frac{\partial}{\partial t}\psi(x,t), \tag{1}$$

where $V(x)$ represents the whole system potential. To arrive easily to the answer without solving the Eq. (1), we assume the system has been formed by connecting two separated systems (Fig. 1b) which have been brought close together at a later time. According to Bardeen theory, we assume that we know the behaviour of the two subsystems separately. Therefore, we consider φ_m the eigenfunction and E_m the eigenenergy of the first subsystem and ψ_n the eigenfunction and E_n the eigenenergy of the other system as the known solutions of the corresponding Schrödinger equations as follows (Fig. 1b):

$$H_m\varphi_m = -\frac{\hbar^2}{2m}\nabla^2\varphi_m + V_{0l}\varphi_m = E_m\varphi_m, \tag{2}$$

$$H_n\psi_n = -\frac{\hbar^2}{2m}\nabla^2\psi_n + V_{hn}\psi_n = E_n\psi_n, \tag{3}$$

where H_m and H_n represent the Hamiltonian of the two subsystems. Also, we define V_{0l} and V_{hn}, the potential profiles to be:

$$\begin{aligned} V_1 = V_{0l} = V_{0s} &= \begin{cases} V(x) & 0 \to s \\ 0 & s \to n, \text{ elsewhere} \end{cases} \\ V_2 = V_{hn} = V_{sn} &= \begin{cases} 0 & 0 \to s, \text{ elsewhere} \\ V(x) & s \to n \end{cases} \end{aligned} \tag{4}$$

where, for simplicity, we have assumed the arbitrary points, l and h, showing the same point called s. Let us suppose the particle initially occupies the subsystem 'n', so we can write down $\psi(x,t)$ the whole system wave function as follows [17]:

$$\psi(x,t) = e^{-\frac{iE_nt}{\hbar}}\psi_n + \sum a_m(t)\varphi_m \tag{5}$$

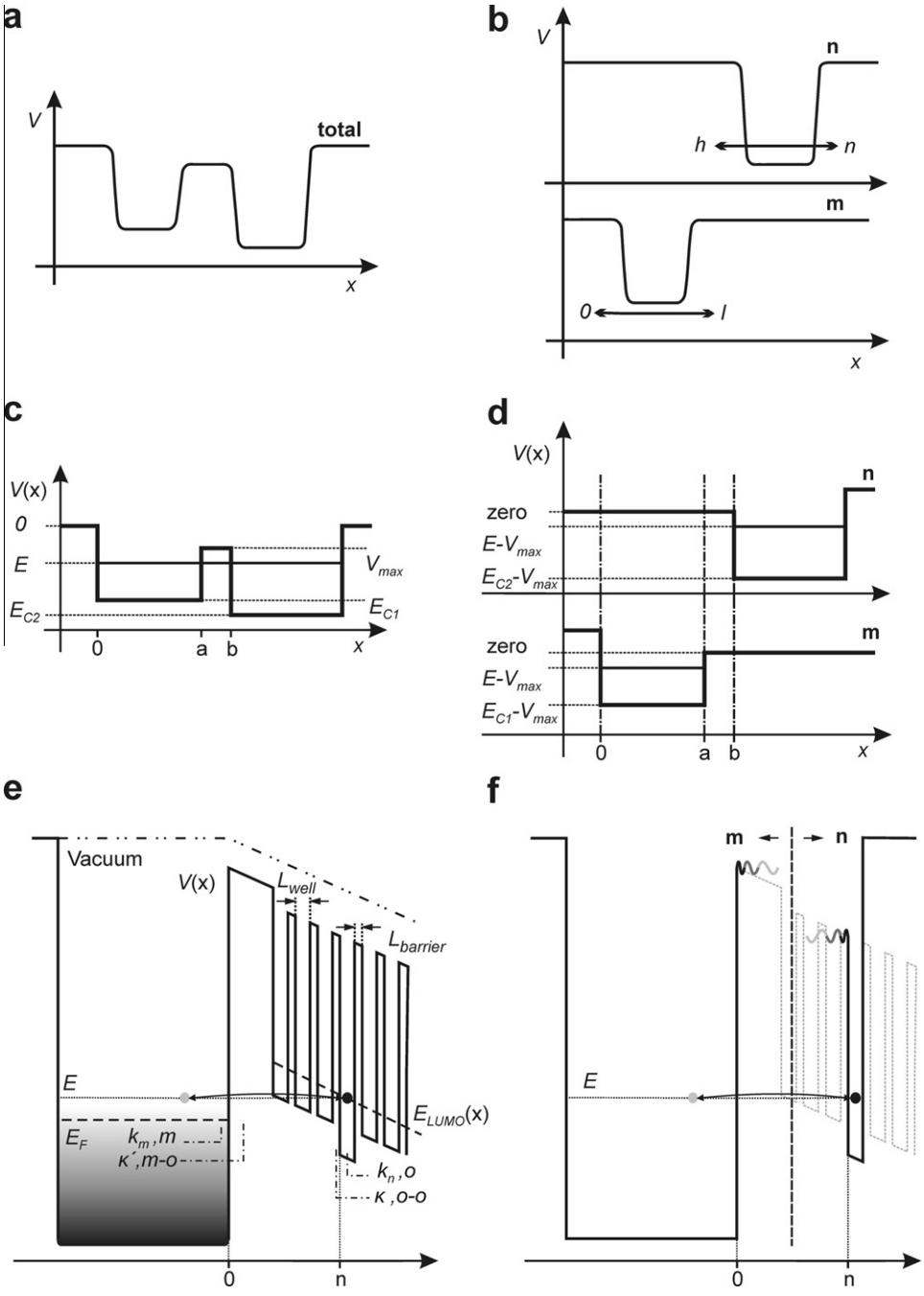

Fig. 1. Potential profiles which are used to explain the Bardeen tunnelling theory and to derive the relation formulating the injection of carriers in metal–organic interfaces. (a) A potential profile including a barrier. The barrier separates the profile into two parts. Initially, we place a particle in one side. The objective is to determine the transmission of the particle to the other side. (b) The potential profile is divided into two subsystems following the Bardeen theory. (c) A one-dimensional potential profile representing a contact between two solids with band-like extended states. (d) According to Bardeen theory, we separate the tunnelling system into two subsystems to calculate the transmission rate. (e) The proposed energy potential profile for a metal–organic interface. Note the width and height of the barriers and wells are not sketched in scale. (f) Dividing the potential profile of metal–organic contact into two subsystems to calculate carrier transmission, the subsystem *m* represents the metal side and the subsystem *n* shows the semiconductor side.

By taking the product of $<\varphi_m|$ in ψ above Eq. (5), we can approximately calculate $d|a_m(t)|^2/dt$ the carrier transmission rate between the subsystems '*n*' and '*m*'. In calculation, we employ the whole system time-dependent Schrödinger Eq. (1) and we assume φ_m and ψ_n are nearly orthogonal. Finally, we obtain [16,17,20]:

$$\frac{d}{dt}|a_m(t)|^2 = \frac{2\pi}{h}M^2\{f_m(1-f_n) - f_n(1-f_m)\}\delta(E_m - E_n), \quad (6)$$

where $M^2 = |\langle\varphi_m|H - H_n|\psi_n\rangle|^2$ the matrix element plays a key role in the transmission rate calculation and f_i is the Fermi–Dirac distribution function of the subsystem '*i*'. Taking into account that ψ_n and its derivative vanishes inside the other subsystem '*m*', we can write the matrix element as [22,16]:

$$M = \int \varphi_m^*(H - H_n)\psi_n dx = -\frac{\hbar^2}{2m}\left[\varphi_m^*\frac{\partial}{\partial x}\psi_n - \psi_n\frac{\partial}{\partial x}\varphi_m^*\right]\Big|_{x=s}. \tag{7}$$

The next step is to evaluate the matrix element. In Section 3, we calculate the *M* for a simple case and we compare the result with the standard tunnelling method.

3. Comparing Bardeen tunnelling method with the standard tunnelling theory

Fig. 1c pictures the potential profile used to compare the results of the two tunnelling methods. This profile for instance can represent the contact between two conductors. In standard tunnelling theory, we start the calculation by writing the wave function as follows:

$$\psi(x) = \begin{cases} Ae^{ik_1x} + Be^{-ik_1x} & x \le a \\ Ce^{\kappa x} + De^{-\kappa x} & a \le x \le b \\ Ee^{ik_2x} + Fe^{-ik_2x} & b \le x \end{cases}, \tag{8}$$

where $k_1 = (2m_e(E - E_{c1})/\hbar^2)^{1/2}$, $\kappa = (2m_e(V_{max} - E)/\hbar^2)^{1/2}$, and $k_2 = (2m_e(E - E_{c2})/\hbar^2)^{1/2}$. E is the carrier energy, m_e the carrier mass, and $\hbar$ the Planck constant divided by 2π. The parameters E_{c1}, E_{c2}, and V_{max} describe the potential profile and are marked in Fig. 1c. Taking into account the continuity of the wave function and its derivative; we can calculate the coefficient A in terms of coefficients E and F [23]:

$$\begin{aligned} A = &+\frac{1}{4}e^{-ik_1a+ik_2b}\left(1+\frac{\kappa}{ik_1}\right)\left(1+\frac{ik_2}{\kappa}\right)e^{-\kappa(b-a)}E \\ &+\frac{1}{4}e^{-ik_1a+ik_2b}\left(1-\frac{\kappa}{ik_1}\right)\left(1-\frac{ik_2}{\kappa}\right)e^{\kappa(b-a)}E \\ &+\frac{1}{4}e^{-ik_1a-ik_2b}\left(1+\frac{\kappa}{ik_1}\right)\left(1-\frac{ik_2}{\kappa}\right)e^{-\kappa(b-a)}F \\ &+\frac{1}{4}e^{-ik_1a-ik_2b}\left(1-\frac{\kappa}{ik_1}\right)\left(1+\frac{ik_2}{\kappa}\right)e^{\kappa(b-a)}F. \end{aligned} \tag{9}$$

We suppose the particle initially occupies the left side of the potential; therefore, F vanishes and the transmission coefficient from the left to the right side becomes:

$$\begin{aligned} T^{-1} &= \left(\frac{E}{A}\right)^{-1}\left(\frac{k_2}{k_1}\right)^{-1/2} \\ &= \left\{+\frac{1}{4}e^{-ik_1a+ik_2b}\left(1+\frac{\kappa}{ik_1}\right)\left(1+\frac{ik_2}{\kappa}\right)e^{-\kappa(b-a)}\right. \\ &\quad \left.+\frac{1}{4}e^{-ik_1a+ik_2b}\left(1-\frac{\kappa}{ik_1}\right)\left(1-\frac{ik_2}{\kappa}\right)e^{\kappa(b-a)}\right\}\left(\frac{k_2}{k_1}\right)^{-1/2}. \end{aligned} \tag{10}$$

If $\kappa(b-a) > 1$, then the transmission probability reduces to:

$$|T|^2 = \left|\frac{E}{A}\right|^2\left|\frac{k_2}{k_1}\right| = \frac{(4\kappa)^2k_1k_2e^{-2k(b-a)}}{(k_1k + k_2k)^2 + (k_1k_2 - k^2)^2}, \tag{11}$$

and for $k = k_1 = k_2$, it ends to:

$$|T|^2 = \left|\frac{E}{A}\right|^2\left|\frac{k_2}{k_1}\right| = \frac{(4k\kappa)^2e^{-2\kappa(b-a)}}{(k^2+\kappa^2)^2}. \tag{12}$$

On the other hand, to calculate the matrix element for the Bardeen theory, the system is separated into two subsystems (Fig. 1d). We write down the wave functions φ_m and ψ_n in a middle point within the potential barrier called *s*, by using:

$$\begin{aligned} \varphi_m(x) &= \begin{cases} A\exp(ik_1x) + B\exp(-ik_1x) & 0 < x < a \\ D\exp(-\kappa x) & a < x \end{cases} \\ \psi_n(x) &= \begin{cases} E\exp(ik_2x) + F\exp(-ik_2x) & x > b \\ C\exp(\kappa x) & b > x > 0 \end{cases}, \end{aligned} \tag{13}$$

where we have vertically shifted the potential profile to simplify the calculation (Fig. 1d). By considering the continuity of the wave function and its derivative at the proper points, we can calculate the coefficients D and C in terms of the coefficients A and F, respectively:

$$D = 2e^{ik_1a+\kappa a}\frac{ik_1}{ik_1 - \kappa}A, \quad C = 2e^{ik_2b-\kappa b}\frac{ik_2}{ik_2 - \kappa}F, \tag{14}$$

Therefore, M^2 becomes:

$$\begin{aligned} M^2 = &\left(-\frac{\hbar^2}{2m}\right)(2\kappa)^2|F|^2|A|^2 \\ &\times\left(\frac{(4k_1k_2)^2}{(\kappa^2+k_1k_2)^2+\kappa^2(k_2-k_1)^2}\right)\exp(-2\kappa(b-a)), \end{aligned} \tag{15}$$

and for $k = k_1 = k_2$, it leads to:

$$M^2 = \left(-\frac{\hbar^2}{2m}\right)^2\left(\frac{(4\kappa k)^2e^{-2\kappa(b-a)}}{(\kappa^2+k^2)^2}\right)(2k)^2|F|^2|A|^2. \tag{16}$$

The term $(4\kappa k)^2\exp(-2\kappa(b-a))/(\kappa^2+k^2)^2$ has been appeared in both M^2 and $|T|^2$ indicating the analogy between the two methods. However, by employing the Bardeen theory, one can directly obtain the time dependency of the carrier transmission.

In Section 4, we apply the Bardeen theory to treat the carrier injection across an m–o/p contact.

4. Current carrier injection at a metal–organic interface

Fig. 1e sketches schematically the potential profile, which governs the carrier dynamics in an m–o/p contact. Naturally, a barrier appears between the electrode and the organic solid. Furthermore, the localized nature of the carriers in the organic semiconductor implies that they are confined in potential wells in the organic material. Consequently, there are narrow barriers between each pair of sites in the one-dimensional model of the organic semiconductor preventing from extended-state formation. Therefore, an injected carrier should tunnel through these barriers to get to the destination node. The proposed potential profile includes the main features of the contact, which are necessary to investigate the injection. According to the Bardeen theory, to determine the dynamics of the particle, it is enough to specify the wave functions of the

two subsystems at one point within the barrier. Therefore, first, we divide the contact potential into two parts exactly next to the organic node which is the destination of the injected carrier. Again, we name the wave functions representing the electrode and the organic part as φ_m and ψ_n, respectively (see Fig. 1f). In one dimension, we can express these functions in terms of plane waves. At entering points into the barrier, the wave functions equal:

$$\begin{aligned}\varphi_m(x) &= \begin{cases} A\exp(ik_m x) + B\exp(-ik_m x) & x:0^- \\ D\exp(-\kappa' x) & x:0^+ \end{cases} \rightarrow \varphi_m(x)|_{0^+} \\ &= 2\left(\frac{ik_m}{ik_m-\kappa'}\right)Ae^{ik_m a+\kappa' a}e^{-\kappa' x}(a\rightarrow 0) \\ \psi_n(x) &= \begin{cases} E\exp(ik_n x) + F\exp(-ik_n x) & x:x_n^+ \\ C\exp(\kappa x) & x:x_n^- \end{cases} \rightarrow \psi_n(x)|_{x_n^-} \\ &= 2\left(\frac{ik_n}{ik_n-\kappa}\right)Fe^{-ik_n b-\kappa b}e^{-\kappa x}(b\rightarrow x_n), \end{aligned} \tag{17}$$

where k_m , k_n, κ, and κ' denote carrier wave numbers in the electrode, in the organic node, in the space between two nodes inside the organic solid, and within the physical barrier respectively. Nevertheless, by some algebraic manipulation, we can evaluate the both wave functions at one point, namely x_n^-. If the potential altitude remained unchanged through the barrier region, the wave function amplitude would decay exponentially:

$$\varphi_m(x_n^-)/\varphi_m(0^+) = e^{-\kappa' L}, \tag{18}$$

where L is the barrier width. However, the barrier does not obey a known curvature. To calculate how the φ_m decays from 0^+ to x_n^-, we can separately consider the effect of the narrow barriers and the slow variation of the potential. Therefore, by using the JWKB approximation and neglecting the back-flowing wave function, we can write:

$$\begin{aligned}\varphi_m(x_n^-)/\varphi_m(0^+) =& \alpha'\alpha^{n-1}\exp(i\Delta)\exp \\ &\times\left(-\int_0^{x_n} dx'\sqrt{\frac{2m_e}{\hbar^2}(V'(x')-E)}\theta(V'(x')-E)\right),\end{aligned} \tag{19}$$

where V' represents the potential profile without the narrow barriers and E is the tunnelling energy and Δ the total phase shift. Also, α shows the amplitude attenuation caused by passing through the narrow barriers in the organic material. α equals $\exp\{-\hbar^{-1}(2m_e(V_{0-0}^{\text{barrier}}\text{-}E)^{1/2})(L_{0-0}^{\text{barrier}})\}$ in which m_e is the electron mass, V_{0-0}^{barrier} the altitude of the internal effective barrier between organic molecules, and L_{0-0}^{barrier} (L^{barrier} in the Fig. 1e) the width of the barrier. The term α' is the same as $\exp(-\kappa(b-a))$ in relation (15) and represents the attenuation caused by the barrier between the metal and the organic solid. Plugging ψ_n and φ_m into the Eq. (7) leaves:

$$\begin{aligned}M^2 =& \left(\frac{-\hbar^2}{2m}\right)^2(\kappa+\kappa')^2|F|^2|A|^2 \\ &\times\frac{(4k_m k_n)^2}{(\kappa\kappa'+k_m k_n)^2+(\kappa k_m-\kappa' k_n)^2} \\ &\times(\alpha')^2(\alpha^{n-1})^2\exp(-2d(x_n)),\end{aligned} \tag{20}$$

where $d(x_n) = \int dx'\hbar^{-1}(2m_e(V'(x')-E))^{1/2}\theta(V'(x')-E)$ is an integration from 0 to x_n. The term $\exp(-2d(x_n))$ includes the effect of slow variation in potential profile caused by external filed, space charges, and image potential and so on. We have substituted 2κ by $(\kappa+\kappa')$, because the calculation using ψ_n leads to $2\kappa'$. Finally, we can write the rate of the carrier injection into the nth layer inside the organic solid as follows:

$$\begin{aligned}&\frac{d}{dt}n_n = \frac{d}{dt}\sum_m |a_m(t)|^2 = \rho\frac{2\pi}{\hbar}M^2\{f-n_n\} = \nu_n\{f-n_n\}, \\ &\nu_n = \nu_0\alpha^{2n-2}\exp(-2d(x_n)), \\ &\nu_0 = \frac{2\pi}{\hbar}\left(\frac{\rho}{L_{\text{well}}}\right)\left(-\frac{\hbar^2}{2m_e}\right)^2\frac{(4k_m k_n)^2(\kappa+\kappa')^2}{(\kappa\kappa'+k_m k_n)^2+(\kappa k_m-\kappa' k_n)^2}(\alpha')^2,\end{aligned} \tag{21}$$

where ρ is the metal density of states per unit length and L_{well} the carrier delocalization length in the organic semiconductor. The term ν_n has the unit of s^{-1} and expresses the hopping rate into the nth layer inside the organic material. This quantity and in particular ν_0 play important role in models describing the injection in organic devices. In Section 4, we will quantitatively calculate the hopping frequency for the contact between polyfluorene (PFO) and some conductors. We would like to mention our model is largely inspired by the one developed by Bussac and Zuppiroli at EPFL Lausanne [15,24]. However, its originality resides in the use of the Bardeen approach, which allow for estimating the injection of charge carriers deep into the organic semiconductor. This is in a different manner compared with the model proposed by Bässler et al. at Philipps-University Marburg [1,13].

5. Results

To examine the presented injection relation, we calculated the values of ν_0 for contacts in some polyfluorene-based OLEDs. We inserted these values into an OLED numerical code, called MOLED [25], to simulate the J–V characteristics of the devices and compared the results with experimental measurements. To fabricate the devices, poly (9,9-di-*n*-octylfluorenyl-2,7-diyl) (PFO) or poly [(9,9-di-*n*-octylfluoreneyl-2,7-diyl)-alt-(benzo[2,1,3]thiadiazol-4,8-diyl)] (F8BT) was spin-casted onto an anode electrode and then covered by thermal evaporating of aluminium (Al). The thickness of the active polymer was 80–90 nm and of the aluminium cathode electrode more than 250 nm. The anode was comprised of indium tin oxide (ITO) coated poly(ethylene terephthalate) (PET) sheets. We coated a ~60 nm thin layer of poly (3,4-ethylendioxythiophene) (PEDOT):poly(styrenesulfonate) (PSS) onto the ITO layer to facilitate hole injection. All the materials were purchased from Sigma–Aldrich. We recorded the electrical characteristics of the devices by means of a Keithley238 source-measurement unit. Also, the thicknesses of the films were measured using a Dectak profilometer.

Aluminium is a high work-function metal which makes holes to be the dominant carriers in the device. Indeed, the choice of polymers with high ionization potentials implies the devices operate in injection-limited current regime and

Table 1
Parameters used in the model and the hopping frequencies calculated for the blue diode (PFO). E_{LUMO} is the energy of the lowest unoccupied molecular orbital in polymer and E_{HOMO} the energy of the highest occupied molecular orbital [26]. We used E_{LUMO} to calculate α' for injection when carriers leaving the polymer and to calculate κ as well. Also, we considered the Fermi energy in polymer to be $(E_{LUMO} + E_{HOMO})/2$ which used to calculate k_n. We employed the Poole–Frenkel mobility type for polyfluorene [9]. D is the thickness of the active polymer.

Parameter	Value
E_{LUMO}	2.2 eV
E_{HOMO}	5.8 eV
μ_{0_p}	1×10^{-5} cm^2/Vs
μ_{0_n}	3×10^{-6} cm^2/Vs
F_{0_p}	6×10^5 V/cm
F_{0_n}	1×10^7 V/cm
$L_{m-o}^{barrier}$	1.05 nm
α^2	0.3
D	85 nm
$V_0^{Anode-HOMO}$	1.39×10^8 s^{-1}
$V_0^{HOMO-Cathode}$	1.10×10^9 s^{-1}
$V_0^{Cathode-LUMO}$	2.12×10^6 s^{-1}
$V_0^{LUMO-Anode}$	1.27×10^9 s^{-1}

Table 2
Parameters and calculated hopping frequencies for the green diode (F8BT). Note the mobility of carriers in F8BT was assumed to be constant [27].

Parameter	Value
E_{LUMO}	3.3 eV
E_{HOMO}	5.8 eV
μ_{-p}	4×10^{-4} cm^2/Vs
μ_{-n}	1×10^{-4} cm^2/Vs
$L_{m-o}^{barrier}$	0.93 nm
α^2	0.3
D	85 nm
$V_0^{Anode-HOMO}$	7.29×10^7 s^{-1}
$V_0^{HOMO-Cathode}$	3.31×10^9 s^{-1}
$V_0^{Cathode-LUMO}$	2.90×10^7 s^{-1}
$V_0^{LUMO-Anode}$	3.51×10^8 s^{-1}

Table 3
We used the Fermi energies to calculate the Fermi vectors, k_m, and to calculate the density of states in electrodes. Also, we employed the work-functions to calculate κ'.

Parameter	Value (eV)
EFAl	11.7
EFAnode	9.4
WfAl	4.28
WfAnode	5.20

in particular the parameters of the anode-polymer interface control the electrical characteristic of the devices in forward bias. In contrast to devices with small energy barriers in which carriers can jump deep into the semiconductor and space-charge limited current (SCLC) flows through the device. So the role of interface parameters begins to fade and the device characteristic is scaled with other parameters such as the thickness of the polymer film. This situation describes for instance a device based on poly [2-methoxy-5-(2-ethylhexyloxy)-1,4-phenylenevinylene] (MEH-PPV) and shall be investigated elsewhere using our model.

Tables 1 and 2 summarise some parameters we used to model the blue and green devices respectively. Also, Table 3 tabulates the values of the Fermi energies and work-functions of the electrodes. We considered dimers of fluorene units form the charge carriers, so the delocalization length of the carriers (L_{well}) in PFO and also F8BT is set to 1.68 nm as we assumed a line of 12 carbon–carbon bonds and each bond 140 pm long. The interchain distance, however, is fixed at 0.3 nm. Also, we set the barrier width to be around 1 nm. It is worth noting that we obtained similar results by considering slightly different values for these parameters i.e. 0.4 nm for the interchain distance or assuming a trimer of fluorene units forms the charge carrier unit [28]. The calculated hopping frequencies were summarised in Tables 1 and 2 as well. We see the hopping rate of holes from anode electrode to polymers is around 10^{+8} s^{-1} for these devices. Fig. 2a and b compares the results of simulation and experiment for PFO- and F8BT-based devices respectively. The two devices show similar characteristics as the ionization potentials of the polyfluorene and polyfluorene-co-benzothiadiazole are similar (~5.8 eV). It is worth mentioning that we took the values of mobility for the emissive materials from the literature. In particular, we employed the Poole–Frenkel type mobility for PFO [9] whilst we used constant values for the mobility of carriers in F8BT [27] and we see there is a good agreement between experiment and modelling in both cases. It is possible to consider a field-dependent mobility for F8BT-based device as well and obtain reasonable results, however, as we mentioned earlier it is the contact that governs the device characteristic.

As we noted earlier, hopping of carriers has been used to model electrical characteristic in organic devices. Table 4 presents some values of hopping frequencies which have been assumed or calculated to describe injection in OLEDs. In Table 5, we summarise the calculated values according to our model for hopping rate of contacts which were presented in Table 4. We mostly took the values of parameters from the corresponding references to calculate the rates of hopping. For small molecule materials, we assumed the delocalization length to be 0.4 nm [3]. Table 5 shows that hopping rate depends strongly on the width of the barrier, so we need to know the accurate value of the barrier width to be able to determine the hopping frequency precisely and to provide a reasonable judgment.

Now let us investigate the dependency of the hopping frequency on the parameters of the contact. Firstly, we consider the effect of width and height of the barrier. We expect that as the height or width of the physical barrier increases the hopping frequency decreases, which consequently leads in reduction of the injection current. Fig. 3 draws the dependency of v_0 on the height of the barrier for contacts between PFO with three different cathode metals. The graph confirms the reduction in v_0 due to

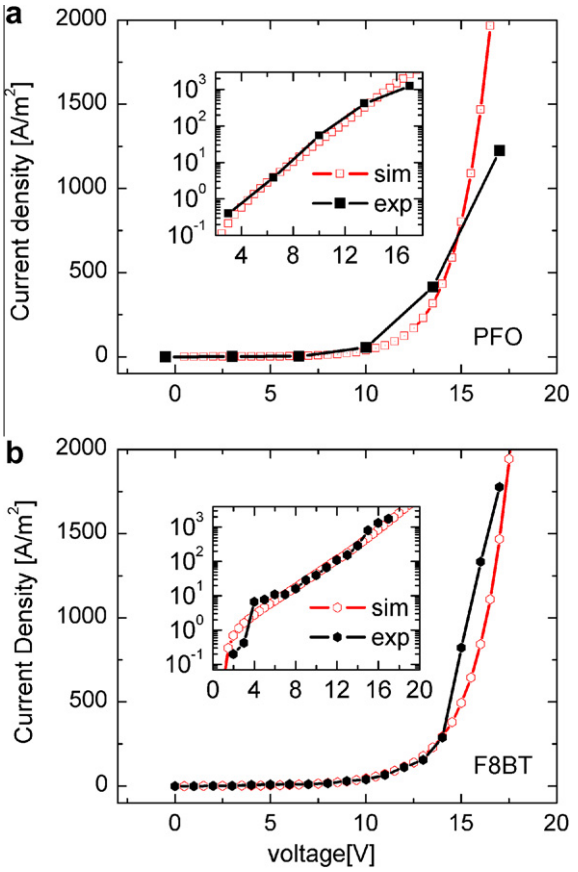

Fig. 2. The J–V characteristics for OLEDs based on PFO (a) and F8BT (b) with Al as the cathode electrode. The curves compare the experiment (filled symbols) with modelling (hollow symbols). The insets represent the results in logarithmic scale. For our green and blue devices the J–V characteristics are quite identical. Note current density is higher than its general trend in low bias voltages (the inset in figure b). Similar discrepancy occurs in PFO-based device; however it is not recorded and presented here. Meng and co-workers showed that one can model this phenomenon by introducing filament conduction into the injection relation [9].

Table 4
The values of hopping rates which have been used in modelling of injection mechanism in OLEDs. The models developed or employed by different authors are not identical. Please see the references for details.

Reference	Contact	Hopping rate (s^{-1})
[9]	Ca/PFO	10^{12}
[14]	Al/Alq_3	10^{13}
[25]	ITO/CuPc	4×10^7
[25]	Al/LiF/Alq_3	4×10^7

expansion of barrier in width and also in height; however, the dependency on width is stronger.

In Section 4, we mentioned the model accounts for direct injection deep into the organic semiconductor. One of the parameters which controls the probability of direct injection beyond the nearest node is α. Fig. 4 shows hopping frequency versus the distance of the nodes from the electrode for different values of α for a contact between

Table 5
Employing the model developed here to calculate the hopping rate for the contacts mentioned in Table 4. The hopping rate strongly depends on barrier width. Yang et al. considered the distance a from the electrode to the first available hopping site in the bulk to be $a = 1.67$ nm [9]. Also, Houili and co-workers considered the separation between the anode and CuPc and also between Alq_3 and the cathode to be 0.33 and 1.33 nm respectively [25]. Moreover, for more appropriate calculation of hopping rate when there is a dipole moment between the organic material and the electrode, for instance a thin layer of LiF, we can replace the square potential barrier with a trapezium one in the calculation of α'.

	0.4 nm	0.7 nm	1.2 nm
Ca/PFO	$1.1 \times 10^{13}\ s^{-1}$	$5.8 \times 10^{10}\ s^{-1}$	$9.9 \times 10^{6}\ s^{-1}$
Al/Alq3	$9.1 \times 10^{12}\ s^{-1}$	$1.6 \times 10^{10}\ s^{-1}$	$3.9 \times 10^{5}\ s^{-1}$
ITO/CuPc	$1.6 \times 10^{13}\ s^{-1}$	$4.1 \times 10^{10}\ s^{-1}$	$2.0 \times 10^{6}\ s^{-1}$
Al/LiF/Alq3	$1.8 \times 10^{13}\ s^{-1}$	$5.6 \times 10^{10}\ s^{-1}$	$3.6 \times 10^{6}\ s^{-1}$

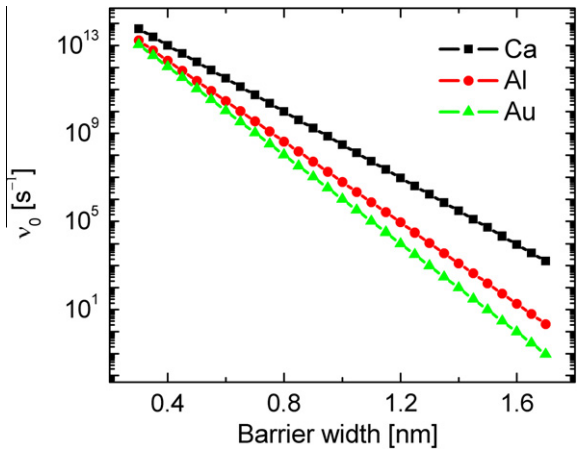

Fig. 3. The dependency of ν_0 on the width and height of the barrier between cathode electrode and the organic semiconductor (i.e. polyfluorene). The hopping rate will change several orders of magnitude if there is an expansion in the width or height of the barrier. We took the values for the work-function from Bernius et al. [29] and for the Fermi vectors and the Fermi energies from Ashcroft and Mermin [30]. We assumed the delocalization length of carriers to be 1.68 nm. For very thin barriers, ν_0 is mostly determined by the width of the barrier; however as we will show in Fig. 5, hopping is restricted to the first few nearest sites when the height of the barrier is considerable.

PFO and PEDOT:PSS with $\varphi_b = 0.6$ eV. Here, we assumed the potential profile without the narrow barriers had a form of $U(x) = \varphi_b - e^2/(16\pi\varepsilon\varepsilon_0 x) - eFx$ where ε_0 is the vacuum permittivity, ε the dielectric constant, e the elementary charge, and φ_b the bare potential barrier. Also, the external electric field, F, was considered to be $2 \times 10^{+6}$ V/cm. From Fig. 4, we see the hopping to the layers beyond the nearest node is not negligible and should be considered especially for the values of α close to one.

Moreover, injection into deep layers inside the organic material is controlled by φ_b and external electric field via the term $\exp(-2d(x_n))$. In Fig. 5, we compare the hopping rate into different layers of the semiconductor for contacts between PFO and different cathode metals. For these contacts, the value of α does not vary as the semiconductor has been kept unchanged whereas φ_b increases as we employ metals with higher work function. Again, a fixed electric field of $2 \times 10^{+6}$ V/cm is considered. The curves in

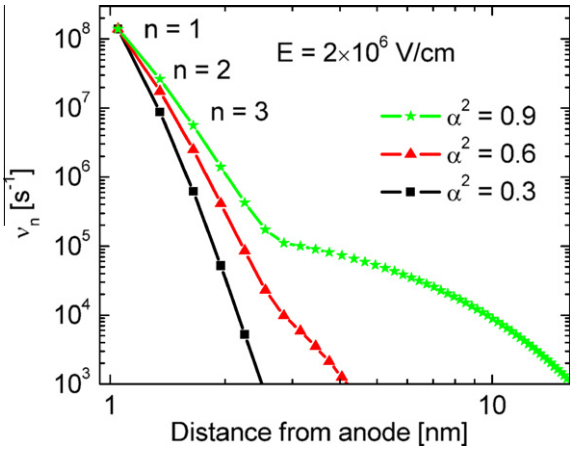

Fig. 4. The hopping rate of carriers into internal layers of the organic semiconductor. We investigated the contact between PFO and PEDOT:PSS with φ_b of 0.6 eV when an external field of 2×10^6 V/cm is applied. Here and in the following figures, we have considered again the interchain distance to be 0.3 nm. For cases in which the barrier is low (φ_b approaches zero) and the carriers inside the organic material are coupled well together (α approaches one), the hopping of the carriers deep into the semiconductor plays significant portion in the injection.

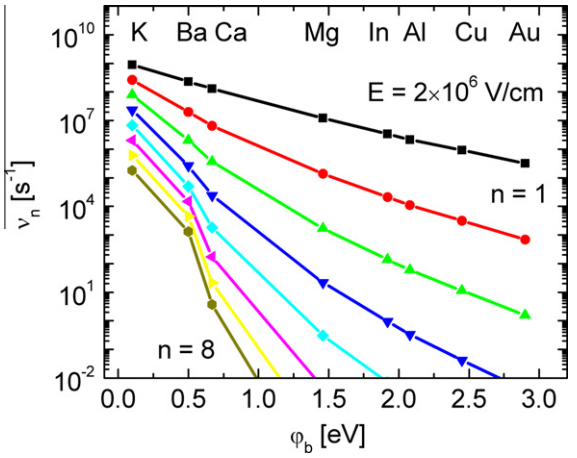

Fig. 5. The hopping rate of electrons into deep layers inside the organic material (ν_n) versus bare potential barrier (φ_b) for PFO in contact with different metals. The match between the E_{LUMO} and the electrode work-function leads in strong coupling between the semiconductor and the metal, even for states deep inside the conjugated polymer. In contrast, a mismatch in energy levels restricts the hopping just to the first few sites of the organic material. For PFO-based device, we assumed the $L_{m\text{-}o}$ to be 1.05 nm.

Fig. 5 suggest high potential barrier restricts the hopping of carriers to the few close layers of the organic material; however, for low barrier contacts, the direct injection into internal layers has significant portion in the current injection.

Finally, we investigate the dependency of hopping rate on the applied bias. We expect the current density increases as we increase the bias voltage. Fig. 6 draws the hopping frequency deep into organic layers versus applied bias for injection of electrons for a contact between F8BT and magnesium (Mg) with potential barrier of $\varphi_b = 0.36$ eV. The figure shows the rate of hopping of carriers deep into organic material grows which leads to an increase in injection current. Nevertheless, the injection current is coupled to the transport of carriers within the organic material via the term n_n as well. Increase in external field hastens the movement of carriers towards the other electrode and causes the carriers leave the region close to the electrode more frequently. This causes that carrier density near the electrode decreases and so carrier injection increases dynamically via the term $f - n_n$.

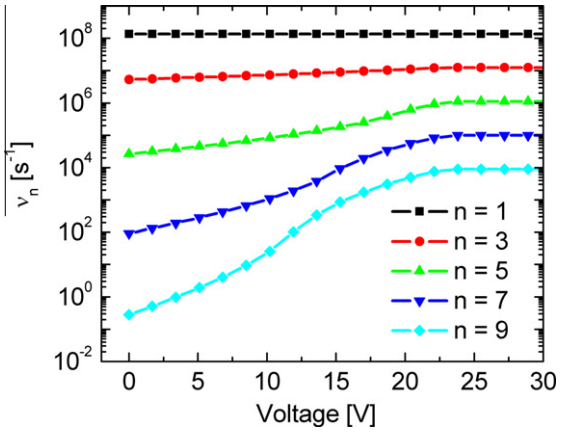

Fig. 6. The ν_n versus applied bias for a contact between F8BT and Mg with φ_b of 0.36 eV. The thickness of the film was considered to be 85 nm and we assumed $L_{m\text{-}o} = 0.93$ nm. For low bias voltages, it is difficult for the carriers to pass through the barrier, they just hop to the few nearest sites; however, as we increase the bias voltage the barrier shrinks and carriers can hop deep into the semiconductor.

6. Conclusion

In present paper, firstly, we introduced the Bardeen tunnelling theory and we presented its correspondence with the standard tunnelling theory. Next, we used the theory to investigate the current carrier across an organic-conductor junction. Then, the model was validated by comparing the simulation results with the experiments for devices with injection-limited current. The parameters in the model were rather theoretical values (like wave numbers); however, the results were in good agreement with the experiments. The main feature of presented model was the insight given about the physics of the injection. In particular, we quantitatively determined the hopping rate of the carriers deep into the organic semiconductor for practical contacts.

Acknowledgements

M.-R. Fathollahi is thankful to Prof. H. Azizi and Prof. H. Mehdian and also M. NateghoIEslam for useful discussions. We would like to thank M. Iraj, Thin Film Laboratories at the University of Tehran for thickness measurements. Also, the authors thank the Mircoelectronics Research and Development Centre of Iran and the research office of the K.N. Toosi University of Technology for financial support.

References

[1] V.I. Arkhipov, E.V. Emelianova, Y.H. Tak, H. Bässler, J. Appl. Phys. 84 (1998) 848.
[2] J. Staudigel, M. Stößel, F. Steuber, J. Simmerer, Appl. Phys. 86 (1999) 3895.
[3] B. Ruhstaller, S.A. Carter, S. Barth, H. Riel, W. Riess, J.C. Scott, J. Appl. Phys. 89 (2001) 4575.
[4] T. Ogawa, D.C. Cho, K. Kaneko, T. Mori, T. Mizutani, Thin Solid Films 438 (2003) 171.
[5] S.J. Martin, A.B. Walker, A.J. Campbell, D.D.C. Bradley, J. Appl. Phys. 98 (2005) 063709.
[6] A. Köhler, H. Bässler, Mater. Sci. Eng. R 66 (2009) 71.
[7] J.C. Scott, J. Vac. Sci. Technol. A 21 (2003) 521.
[8] B. Masenelli, D. Berner, M.N. Bussac, F. Nüesch, L. Zuppiroli, Appl. Phys. Lett. 79 (2001) 4438.
[9] C.-K. Yang, C.-M. Yang, H.-H. Liao, S.-F. Horng, H.-F. Meng, Appl. Phys. Lett. 91 (2007) 093504.
[10] C. Shen, A. Kahn, J. Schwartz, J. Appl. Lett. 89 (2001) 449.
[11] P.W.M. Blom, M.C.J.M. Vissenberg, Mater. Sci. Eng. 27 (2000) 53.
[12] M.N. Bussac, D. Michoud, L. Zuppiroli, Phys. Rev. Lett. 81 (1998) 1678.
[13] V.I. Arkhipov, U. Wolf, H. Bässler, Phys. Rev. B 59 (1999) 7514.
[14] M.A. Baldo, S.R. Forrest, Phys. Rev. B 64 (2001) 085201.
[15] D. Berner, H. Houili, W. Leo, L. Zuppiroli, Phys. Status. Solidi. A 202 (2005) 9.
[16] A.D. Gottlieb, L. Wesoloski, Nanotechnology 17 (2006) 57.
[17] J. Bardeen, Phys. Rev. Lett. 6 (1961) 57.
[18] J. Tersoff, D.R. Hamann, Phys. Rev. Lett. 50 (1983) 1998.
[19] C.J. Chen, Phys. Rev. Lett. 65 (1990) 448.
[20] A. Nitzan, Annu. Rev. Phys. Chem. 52 (2001) 681.
[21] R. Clerc, G. Ghibaudo, G. Pananakakis, Solid-State Electron. 46 (2002) 1039.
[22] M.R. Fathollahi, M.J. Sharifi, H. Mehdian, Proc. 15th Iranian Conf. Elect. Eng., ICEE (2007).
[23] E. Merzbacher, Quantum Mech., second ed., JohnWiley & Sons, Inc., New York, 1998.
[24] E. Tutiš, M.N. Bussac, B. Masenelli, M. Carrard, L. Zuppiroli, J. Appl. Phys. 89 (2001) 430.
[25] H. Houili, E. Tutiš, H. Lütjens, M.N. Bussacc, L. Zuppiroli, Comp. Phys. Commun. 156 (2003) 108.
[26] X. Gonga, D. Mosesa, A.J. Heeger, S. Xiao, Synth. Met. 141 (2004) 17.
[27] Z. Zheng, K.-H. Yim, M.S.M. Saifullah, M.E. Welland, R.H. Friend, J.-S. Kim, W.T.S. Huck, Nano Lett. 7 (2007) 987.
[28] S. Athanasopoulos, J. Kirkpatrick, D. Martnez, J.M. Frost, C.M. Foden, A.B. Walker, J. Nelson, Nano Lett. 7 (2007) 1785.
[29] M.T. Bernius, M. Inbasekaran, J. O'Brien, W. Wu, Adv. Mat. 12 (2000) 1737.
[30] N.W. Aschroft, N.D. Mermin, Solid-State Phys., Harcourt Inc., Orlando, 1976.